Cyclotron decay time of a two-dimensional electron gas from 0.4 to 100 K

Jeremy A. Curtis,[1] Takahisa Tokumoto,[1] A. T. Hatke,[2] Judy G. Cherian,[2] John L. Reno,[3] Stephen A. McGill,[2] Denis Karaiskaj,[4] and David J. Hilton[1,*]

[1]*Department of Physics, University of Alabama at Birmingham, Birmingham, Alabama 35294-1170, USA*
[2]*National High Magnetic Field Laboratory, Florida State University, Tallahassee, FL 30201, USA*
[3]*Center for Integrated Nanotechnologies, Sandia National Laboratory, Albuquerque, New Mexico 87185, USA*
[4]*Department of Physics, University of South Florida, Tampa, Florida 33620, USA*

(Received 2 July 2015; revised manuscript received 29 March 2016; published 29 April 2016)

We have studied the cyclotron decay time of a Landau-quantized two-dimensional electron gas as a function of temperature (0.4–100 K) at a fixed magnetic field (±1.25 T) using terahertz time-domain spectroscopy in a gallium arsenide quantum well with a mobility of $\mu_{dc} = 3.6 \times 10^6\,\mathrm{cm^2\,V^{-1}\,s^{-1}}$ and a carrier concentration of $n_s = 2 \times 10^{11}\,\mathrm{cm^{-2}}$. We find a cyclotron decay time that is limited by superradiant decay of the cyclotron ensemble and a temperature dependence that may result from both dissipative processes as well as a decrease in n_s below 1.5 K. Shubnikov–de Haas characterization determines a quantum lifetime, $\tau_q = 1.1$ ps, which is significantly faster than the corresponding dephasing time, $\tau_s = 66.4$ ps, in our cyclotron data. This is consistent with small-angle scattering as the dominant contribution in this sample, where scattering angles below $\theta \leqslant 13^\circ$ do not efficiently contribute to dephasing. Above 50 K, the cyclotron oscillations show a strong reduction in both the oscillation amplitude and lifetime that result from polar optical phonon scattering.

DOI: 10.1103/PhysRevB.93.155437

I. INTRODUCTION

The gallium arsenide two-dimensional electron gas (2DEG) in a quantum well has long been used as a model system to study the fundamental limits of electronic transport [1–6]. New device geometries that exploit quantum interference in these samples provide an additional degree of freedom that is increasingly important as devices with ever-smaller feature sizes are developed [7,8]. These may also form the basis of next-generation quantum logic provided electron coherence lifetimes that are sufficiently long can be achieved [9]. Existing lifetimes in two-dimensional electron systems (2DES) are sufficient to demonstrate prototype electronic and optical control of coherence [9–11], but there is significant interest in extending these decoherence times to enable new applications. Recent work [12] has shown that the electronic properties of 2DES are influenced by many-body effects including superradiant emission, which emerges only in the highest-mobility samples where the decoherence times are on the same order as or longer than the superradiant emission time. The understanding and mitigation of decoherence in these high-quality 2DES thus may enable a wider array of device geometries based on new phenomena in semiconductor systems, while the development and characterization of high-mobility materials with even longer coherence lifetimes will determine the feasibility of these for device applications.

In this paper, we study the temperature dependence of the cyclotron resonance decay time τ_{CR} in a high-mobility gallium arsenide quantum well two-dimensional electron gas at ±1.25 T from 0.4 to 100 K using terahertz time-domain spectroscopy. Our results show a monotonic decrease in τ_{CR} from 0.4 to 100 K that is limited by the superradiant decay time of the cyclotron ensemble at the lowest temperatures measured [12]. We see a significant decrease in oscillation amplitude A and τ_{CR} above 50 K that is due to strong polar optical phonon scattering in gallium arsenide that results in rapid ensemble dephasing. Below 1.5 K, we also see a decrease in A that is a signature of a decrease in cyclotron population or a reduction in the transition dipole matrix element. Our Shubnikov–de Haas characterization of the same sample determines a quantum lifetime, $\tau_q = 1.1$ ps, which is significantly shorter than either the transport lifetime, $\tau_{DC} = 140$ ps, or the component of τ_{CR} due to scattering, $\tau_s(T) = 66.4$ ps. The temperature dependence of τ_{CR} results from both dissipative processes (i.e., acoustic phonon scattering, polar optical phonon scattering, and impurity scattering [13,14]) and, potentially, a temperature-dependent reduction in free-carrier concentration with a concomitant increase in the superradiance decay time [12].

II. BACKGROUND

Cyclotron resonance is a well-established experimental technique that measures the temperature and magnetic field dependence of the electronic and optical properties in bulk [15] and quantum-confined semiconductors [16–19]. The magnetic field, $\vec{B} = B_0\hat{z}$, splits the density of states into quantized Landau levels separated by the cyclotron energy ($h\nu_c = \hbar e B_0/m^*$) [20,21]. In the experimental data acquired in these experiments, the resonance frequency ν_c determines the effective mass m^* in the two-dimensional layer, while the linewidth $\Delta\nu$ and amplitude A are both functions of τ_{CR} and the carrier concentration n_s [18].

Cyclotron resonance has been extensively used to study the dynamic properties of two-dimensional electron systems in external magnetic fields, primarily in samples with $\mu_{dc} \leqslant 10^5\,\mathrm{cm^2\,V^{-1}\,s^{-1}}$, and has demonstrated a number of novel effects as a function of temperature and magnetic field. The authors of Ref. [16] observed a filling-factor-dependent change in the cyclotron resonance linewidth at 5 K that they modeled assuming reduced intra-Landau-level scattering when

*dhilton@uab.edu

E_F is between Landau levels. A series of cyclotron resonance experiments in samples with a range of mobilities from $\mu_{dc} = 1.2 \times 10^5$ to 1×10^6 cm^2 V^{-1} s^{-1} similarly observed linewidth maxima at even filling factors due to impurity scattering as well as several rational fractions due to reduced screening, although the linewidth oscillations were more prominent in the lower-mobility samples [22].

The effects of strong Coulomb repulsions were first observed as an anomalous shift in the cyclotron resonance frequency due to an enhancement in the effective mass in a sample with $\mu_{dc} = 6.7 \times 10^4$ cm^2 V^{-1} s^{-1} in Ref. [23]. Subsequent investigations with higher-mobility samples ($\sim 10^5$ cm^2 V^{-1} s^{-1}) in Ref. [17] reported a similar redshift in the cyclotron frequency and demonstrated that it can be controlled by both the carrier concentration and external magnetic field. Reference [18] studied a range of carrier concentrations for 1.55×10^{10} to 1.0×10^{11} cm^{-2} in a sample with a mobility of 3×10^5 cm^2 V^{-1} s^{-1} and determined a τ_{CR} of 104 ps at a filling factor of $\nu = 0.4$. The authors note, however, the *absence* of cyclotron resonance linewidth oscillations, which they attribute to the saturation of the intensity transmission linewidth in high-mobility samples ($\gtrsim 10^5$ cm^2 V^{-1} s^{-1}), which eventually becomes independent of any change to τ_{CR}. Subsequent investigations of high-mobility 2DEGs have also established a limiting role of superradiant emission on this resonance lifetime, in addition to the previously discussed role of the saturation of the dissipative processes [12,24]. Because of this saturation effect and the onset of significant superradiant emission, however, few systematic investigations of τ_{CR} have been performed with $\mu_{dc} \geqslant 10^5$ cm^2 V^{-1} s^{-1}.

III. EXPERIMENTAL METHODS

Terahertz time-domain spectroscopy is a new implementation of cyclotron resonance that uses broadband subpicosecond terahertz pulses and a fixed $\vec{B}$ [26–30] instead of a fixed wavelength source with a variable $\vec{B}$ [17,18]. Prior generations of cyclotron resonance experiments measured the intensity of the transmitted far-infrared or terahertz light and have known limitations in the highest-mobility samples. The resonance linewidth $\Delta\nu$ saturates in samples with $\mu_{dc} \geqslant 10^5$ cm^2 V^{-1} s^{-1} and does not unambiguously determine τ_{CR} (see Ref. [18] for a further discussion of this "saturation effect"). Phase-sensitive detection methods, which we employ in our experiments, can directly determine the frequency-dependent real and imaginary dielectric constants [$\tilde{\chi}(\nu)$ in this paper] in a single experimental measurement and thus overcome these limitations [26,27,29].

Figure 1(a) shows a diagram of our cyclotron resonance experiment. An 800-nm pulse from a titanium:sapphire laser amplifier (Coherent Legend) with a duration of 0.150 ps and an energy of 0.6 mJ is used to produce near-single-cycle terahertz pulses by optical rectification in 1-mm-thick (110)-oriented zinc telluride (Ingcrys Laser Systems) [31]. The resulting pulse is linearly polarized ($\vec{E} = E_0\hat{x}$) with a spectrum of frequencies from 0.2 to 1.2 THz. The terahertz pulse has a fluence of $\ll 1$ nJ cm^{-2} and results in negligible sample heating in all of our experiments. This terahertz pulse is normally incident ($\theta = 0$) on the 2DEG sample in a 10-T superconducting magnet (Oxford Instruments SpectroMag) with $\vec{B} \parallel \vec{k}$, where $\vec{k} = \kappa\hat{z}$

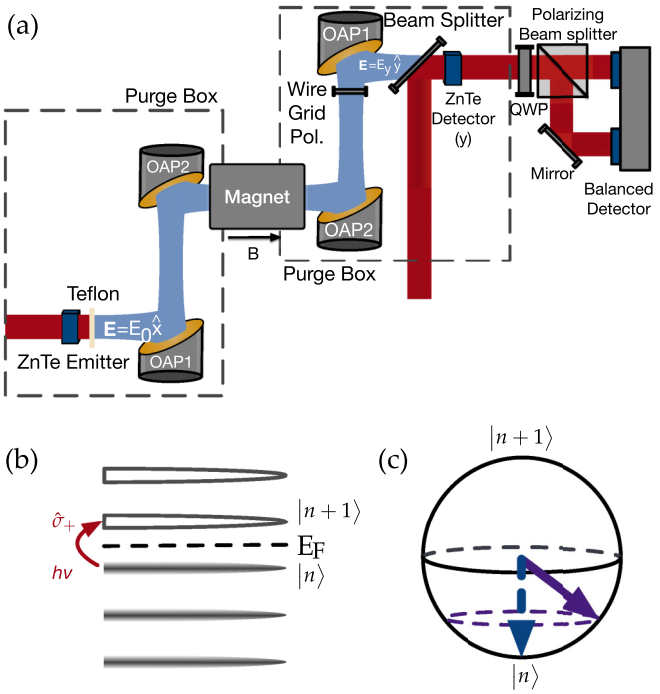

FIG. 1. (a) The apparatus used in the experiments and described in this paper is shown here [25]. Both the emitter and detector are zinc telluride (ZnTe), emitting linearly polarized terahertz pulses $\hat{x}$. The detector is aligned to measure the cross-polarized component $\hat{y}$ of the terahertz electric field that is generated by $\vec{B}$. OAP = off-axis parabolic mirror, QWP = quarter wave plate. (b) The application of an external magnetic field results in the formation of a spectrum of discrete Landau levels separated by the cyclotron energy $h\nu_c$. Adjacent levels have dipole-allowed optical transitions coupled by a circular polarized component of electromagnetic field [20,21]. This results in both circular dichroism (elliptical polarization) and circular birefringence (polarization rotation) in the 2DEG and modifies the polarization of the transmitted terahertz pulse near ν_c. (c) A Bloch sphere representation of the two-level system model used to describe our experiments, where the south pole is the highest filled Landau level $|n\rangle$ and the north pole is the lowest unfilled level $|n+1\rangle$.

is the propagation vector of the terahertz pulse and the 2DEG is the $\hat{x}$-$\hat{y}$ plane. This magnet has a helium-3 cryostat and a base temperature of 0.4 K.

A 2DEG in a perpendicular magnetic field results in a transmitted terahertz pulse that is elliptically polarized with components along both $\hat{x}$ and $\hat{y}$ due to the magnetic-field-induced circular dichroism. We use standard electro-optic sampling techniques to record the amplitude and phase of one linearly polarized component of the transmitted pulse [32]. The polarization axis ($\hat{y}$) of the detector is aligned to measure the cross-polarized component induced by the applied magnetic field. To improve the polarization extinction of this detector configuration, we also align a wire grid polarizer (Microtech Instruments, Model G30) along the $\hat{y}$ direction. This entire experiment is performed in a dry nitrogen atmosphere to minimize the effects of atmospheric water vapor absorption on our data [33].

Our experiments study a 30-nm-thick modulation-doped single GaAs quantum well (sample: EA0745) grown via molecular beam epitaxy. This sample has a carrier

concentration of $n_s = 2 \times 10^{11}\,\mathrm{cm}^{-2}$ and a mobility of $\mu_{dc} = 3.6 \times 10^6\,\mathrm{cm}^2\,\mathrm{V}^{-1}\,\mathrm{s}^{-1}$ at 4.2 K (i.e., a transport scattering time of $\tau_{DC} = 140$ ps).

IV. RESULTS AND DISCUSSION

We measure the terahertz waveform as a function of temperature at $B_0 = \pm 1.25$ T [corresponding to a filling factor of $\nu = 2E_F/(h\nu_c) = 6.6$] and subtract it to isolate the component of the terahertz electric field that demonstrates broken time-reversal symmetry by undergoing a π phase change after magnetic field reversal [34,35]. A representative set of data is shown in Fig. 2(a) for ± 1.25 T at 0.6 K. The time-delayed pulses that appear at multiples of ~15 ps after the initial pulse are additional Fabry-Pérot reflections from the 625-μm gallium arsenide substrate on which the sample is grown. Figure 2(b) shows the subtracted data (offset vertically for clarity) as a function of temperature from 0.4 to 100 K. Our analysis shows an increase in oscillation lifetime as temperature is lowered and a reduction in amplitude below 1.5 K and also above 50 K.

Ultrashort terahertz pulse transmission through a multilayer sample can be modeled using the characteristic matrix method [36,37], which we have previously extended in Ref. [29] to include materials, like in the present study, that are in an external magnetic field. This allows us to model the entire cyclotron resonance signal shown in Fig. 2(b), including the present case when the oscillation decay time is long and there is interference between the multiple reflections [38].

We use a *two-level* system approximation for the susceptibility $\tilde{\chi}(\nu)$ of the cyclotron-active polarization component that results from splitting the density of states near E_F [39]. This approximation neglects all Landau levels except for the highest filled level $|n\rangle$ and lowest unfilled level $|n+1\rangle$ near E_F [shown in Fig. 1(b)] and is appropriate for the dipole $\hat{d}$ transitions that we can access with the low terahertz pulse energies in our experiment. This approximation is valid for our specific excitation conditions but would not be generally applicable if the full Landau spectrum was accessible by the incident field. First, at the lowest temperatures of our experiment, the thermal population in $|n+1\rangle$ is essentially zero (i.e., for $h\nu_c \ll k_B T$). Second, with $|n+1\rangle$ unoccupied, the next unfilled level, $|n+2\rangle$, is only accessible via a quadrupole transition from $|n\rangle$; since the spectral weight of our terahertz pulse is very low at $2\nu_c \approx 1.03$ THz, this will not result in a significant population in any higher-level state. Thus, the only Landau levels that can be addressed by our terahertz excitation at low temperatures are those levels, $|n\rangle$ and $|n+1\rangle$, that are near E_F.

The terahertz pulse results in an ensemble of coherently coupled two-level systems, initially represented as a vector on the Bloch sphere in Fig. 1(c). The dynamical $\tilde{\chi}(\nu)$ of this two-level system in SI units is a homogeneously broadened absorption given by

$$\tilde{\chi}(\nu) = \left(\frac{N|\hat{d}|^2\tau_{CR}}{\epsilon_0\hbar}\right)\left[\frac{i - 2\pi(\nu+\nu_c)\tau_{CR}}{1+4\pi^2(\nu+\nu_c)^2\tau_{CR}^2} - \frac{i - 2\pi(\nu-\nu_c)\tau_{CR}}{1+4\pi^2(\nu-\nu_c)^2\tau_{CR}^2}\right], \quad (1)$$

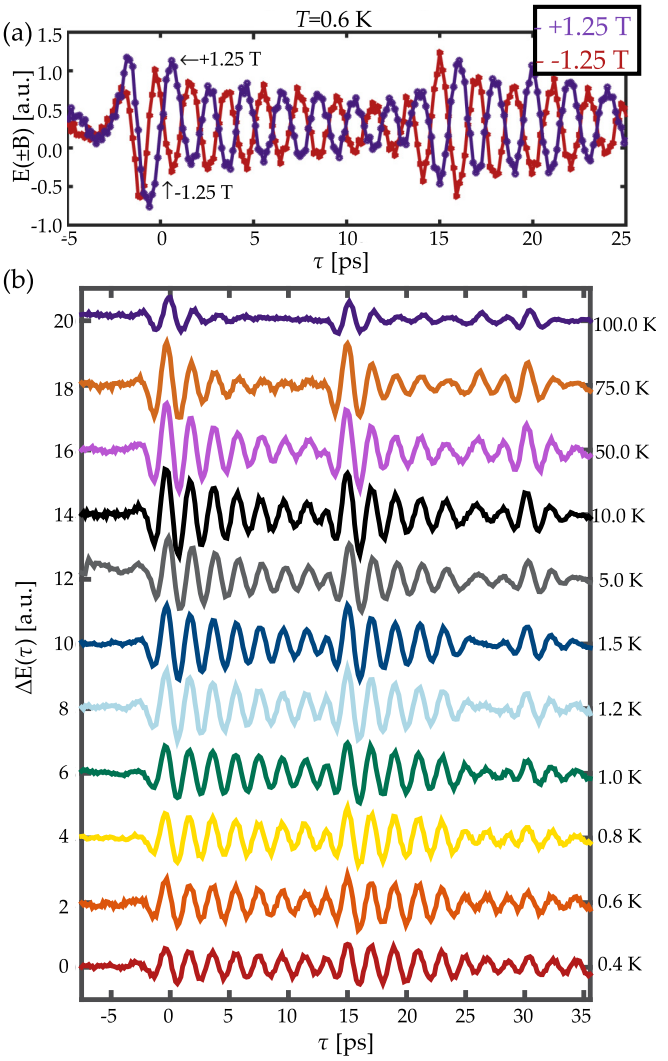

FIG. 2. (a) Cyclotron resonance data $E(\pm B)$ that show oscillations at $B = \pm 1.25$ T and at $T = 0.6$ K. (b) Subtracted cyclotron resonance data, $\Delta E = E(+B) - E(-B)$, for temperatures from 0.4 K (bottom curve) to 100 K (top curve), showing the increase in τ_{CR} at low temperatures. Data shown here at 0.6 K also appear in their subtracted form in (b). The results of the fitting of these data to the multilayer transmission model are described in the text and in Ref. [29] and will be shown in Fig. 3. The secondary pulse located at approximately ~15 ps results from multiple reflections within the GaAs substrate.

where N is the population in $|n\rangle$ before the terahertz pulse excitation and $|\hat{d}|^2$ is the square dipole transition matrix element for the $|n\rangle \rightarrow |n+1\rangle$ transition [39]. The $\epsilon_0\tilde{\chi}(\nu)$ in the frequency domain corresponds to a causal response function $R(t)$ in the time domain that is given by Eq. (2), where IFT is the inverse Fourier transform operation [29,40] and u(t) is the unit step function [41]:

$$R(t) \equiv \mathrm{IFT}[\epsilon_0\tilde{\chi}(\nu)] = \left(\frac{2N|\hat{d}|^2}{\hbar}\right)\mathrm{u}(t)\exp\left(\frac{-t}{\tau_{CR}}\right)\sin 2\pi\nu_c t. \quad (2)$$

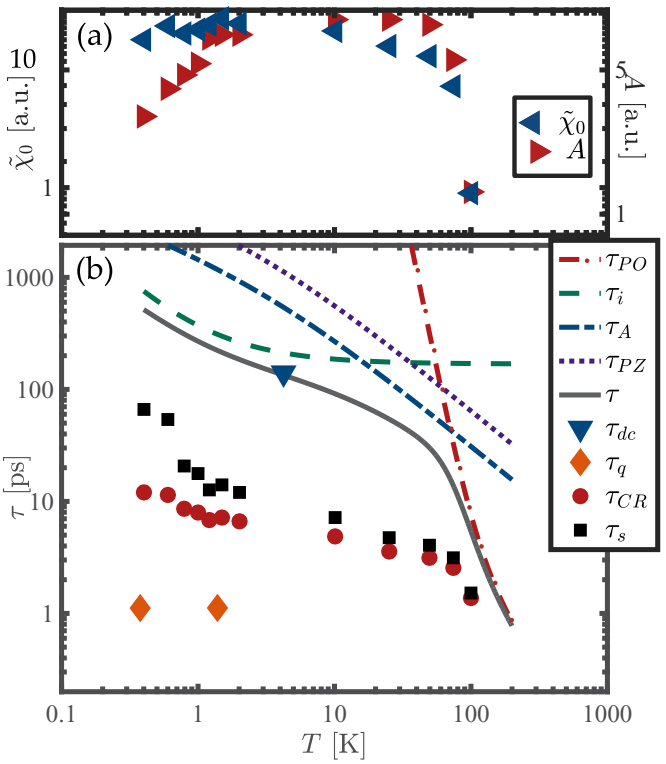

FIG. 3. (a) Rightward-pointing triangles (right axis): The amplitude of the time-domain oscillations A is shown as a function of temperature. Leftward-pointing triangles (left axis): The magnitude of the susceptibility $\tilde{\chi}_0$ is shown as a function of temperature. (b) Circles: The cyclotron lifetime τ_{CR} in EA0745 is shown as a function of temperature, which increases monotonically as the temperature is lowered from 100 to 0.4 K. Triangles: The low-frequency τ_{DC} at 4.2 K was determined using transport characterization techniques. Solid line: The τ_{DC} is calculated using Matthiessen's rule from the individual contributions, using the equations taken from Ref. [42]. Dot-dashed line: The polar optical phonon scattering contribution to τ_{DC} is given by Eq. (31) in Ref. [42]. Dashed line: The combined remote ionized impurity scattering and interface charge contribution to τ_{DC}, which is given by Eqs. (26) and (28) in Ref. [42]. Long- and short-dashed line: The contribution to τ_{DC} due to acoustic phonon scattering is given by Eq. (34) in Ref. [42]. Dotted line: The contribution to τ_{DC} due to piezoelectric scattering is given by Eq. (37) in Ref. [42]. Squares: The temperature-dependent component of τ_{CR}, the result from acoustic phonon, polar optical phonon, and impurity scattering, with a potential second contribution from a reduction in carrier concentration at the lowest temperatures studied [see $A(T)$ in (a)]. Diamonds: The quantum lifetime, $\tau_q = 1.1$ ps, in this sample, which we determine from the Shubnikov–de Haas amplitude decay.

For later use in Fig. 3, we define $\tilde{\chi}_0$ as the maximum value of the imaginary part (absorption) of $\tilde{\chi}$ in Eq. (3a), which occurs at the cyclotron frequency ν_c. Likewise, the peak amplitude of this causal response is given by Eq. (3b) using the same model parameters.

$$\tilde{\chi}_0 = \frac{1}{\epsilon_0 \hbar} N |\hat{d}|^2 \tau_{CR}, \tag{3a}$$

$$A = \frac{2}{\hbar} N |\hat{d}|^2. \tag{3b}$$

We determine the best fit to our data using a constrained genetic algorithm in MATLAB with the characteristic matrix model for $\tilde{t}(\nu)$ and two-level approximation for $\tilde{\chi}(\nu)$. Figure 3(a) shows $\tilde{\chi}_0$ for each of our temperatures (leftward-pointing triangles, left axis), with an approximately temperature-independent behavior below 10 K and a rapid decrease as temperature is increased above 50 K. This is in contrast to the amplitude A, which is also shown in Fig. 3(a) (rightward-pointing triangles, right axis). This amplitude decreases below 1.5 K, which will be discussed in more detail below. We note that the terahertz beam waist at the sample position has a diameter that is comparable to the sample dimensions and probe aperture, which potentially makes our result sensitive to changes in the system alignment. We have verified this does not contribute to the reduction in A below 1.5 K by measuring the transmission through the magnet absent a sample and noting no reduction in signal throughout the temperature range studied.

Figure 3(b) plots τ_{CR} as a function of sample temperature (circles), which monotonically increases as the temperature is lowered from 100 to 0.4 K in our experiments. The cyclotron frequency, $\nu_c = 0.516$ THz, determined in this fitting is consistent with an effective mass of $m^* = 0.0678 m_0$, where m_0 is the free-electron mass. This is within ~0.5% of the accepted value of the effective mass of gallium arsenide [17,43].

In addition to the cyclotron resonance measurements, we also have performed Shubnikov–de Haas measurements. Under a weak perpendicular magnetic field, the low-temperature magnetoresistance ΔR of a 2DES will exhibit well-known Shubnikov–de Haas oscillations (SdHOs) [44] that are periodic in the filling factor, $\nu = 2E_F/\hbar\nu_c$, where E_F and $\hbar\nu_c$ are the Fermi and cyclotron energies, respectively. Resistance minima occur when E_F is in the middle between two cyclotron energy levels. The magnetic field dependence of the amplitude is given by $\Delta R \propto D_T \delta \cos(\pi\nu)$, where $D_T = X_T/\sinh(X_T)$, $X_T = 2\pi^2 k_B T/h\nu_c$, and $\delta = \exp(-\pi/\nu_c\tau_q)$ is the Dingle factor, which we use to extract the quantum scattering time τ_q [45].

In Fig. 4, we show magnetoresistance data (after removal of a slowly varying background) plotted versus ν and observe well-defined SdHOs that monotonically decrease with increasing filling factor. In these magnetic fields and temperatures, the oscillation minima are only observed at even ν, demonstrating an absence of spin splitting, with an amplitude that monotonically decreases with increasing ν. To estimate τ_q, we extract the SdHO amplitude and present the reduced resistance $\Delta R/D_T$ versus ν (circles) on a semilog scale in Fig. 4 (right axis). The amplitude follows an exponential dependence from which we determine the temperature-independent sample average $\tau_q \approx 1.1$ ps (included in Fig. 3 using diamonds). The measured τ_q was found to change by less than 10% over the sample by varying the contact configurations, current directions, and magnetic field orientations.

The amplitude of the cyclotron oscillations A shown in Fig. 3(a) (rightward-pointing triangles) is approximately constant between 1.5 and 50 K, with significant decreases both above and below this range. At the highest temperatures studied, the decrease in A occurs when strong polar optical phonon scattering [2,14] is the main contribution to μ_{dc}. This results in rapid dephasing of the ensemble coherence on a time scale comparable to the terahertz pulse width [46]. The reduction in amplitude A at temperatures below 1.5 K

is a direct measure of the reduction of $N|\hat{d}|^2$, as shown in Eq. (3b) [47], which indicates either a reduction in the population N or a modification to the dipole matrix element $|\langle n|\hat{d}|n+1\rangle|$. The carrier population in this modulation-doped sample originates from the spatially separated δ-doped silicon layer to avoid the problems of freeze-out of carriers that were seen in earlier generations of 2DEGs [48]. Prior investigations of 2DEG samples with *lower* μ_{dc} did not observe the reduction in population that our sample exhibits [18,23]. A full explanation of this reduction in A will require additional experiments to study the temperature, magnetic field, and n_s dependence of cyclotron resonance decay time.

A simplified picture of this experiment is shown in Fig. 5, which models this as three interacting subsystems [49]. The perpendicular external magnetic field generates a set of equally spaced Landau levels in the GaAs 2DEG. Interactions with the lattice will result in a loss of coherence through a combination of impurity, acoustic phonon, and/or polar optical phonon scattering over our temperature range [42]. Finally, the external terahertz field is coupled to the Landau spectrum through inter-Landau-level absorption, which transfers both energy and coherence from the terahertz field to the sample. In high-mobility samples, superradiant emission results in the return of energy and coherence back to the terahertz field. The different lifetimes (τ_s, τ_q, and τ_{SR}) measured in our experiments characterize the observed dynamics in this high-mobility sample. As previously discussed in Ref. [12], Eq. (4b) describes the superradiant emission from the Landau spectrum into the terahertz field, while the inter-Landau terahertz absorption in high-mobility samples has also been extensively studied [27]. In our sample, the coupling to the lattice is on the same order as τ_{SR}, so both the lattice and terahertz field subsystems are coupled to the Landau spectrum and contribute to the observed cyclotron decay.

Coupling between the Landau levels and the terahertz field results both from absorption, which is significantly faster than the temporal resolution of our experimental apparatus, and superradiant decay. The measured cyclotron resonance decay time τ_{CR} is given by

$$\tau_{CR}^{-1} = \tau_{SR}^{-1} + \tau_s(T)^{-1}, \tag{4a}$$

$$\tau_{SR}^{-1} = \frac{e^2 n_s}{\epsilon_0 m^*(1+n_{\mathrm{GaAs}})c}, \tag{4b}$$

where τ_{SR} is the contribution from the superradiant decay of the collective cyclotron ensemble and $\tau_s(T)$ is the additional temperature-dependent component of the decay time. This τ_{SR} is given by Eq. (4b) in SI units, where c is the speed of light, e is the electron charge, and n_{GaAs} is the terahertz frequency refractive index of gallium arsenide [12,50]. This lifetime is $\tau_{SR} = 14.7$ ps in our sample using $n_s = 2\times10^{11}$ cm^{-2} and is a limiting time scale for τ_{CR} at low temperatures in this sample. Using this calculated value of τ_{SR} and our measured τ_{CR} data, we calculate $\tau_s(T)$, which is shown in Fig. 3(b) (squares).

The lifetime τ_s describes the coupling between the Landau levels and the lattice. Two scenarios can explain the observed temperature dependence of $\tau_s(T)$: the temperature dependence of carrier scattering and/or enhanced superradiant emission due to a reduced carrier concentration [see Fig. 3(a)]. For the first scenario, Ref. [12] proposed estimating the scattering contribution to τ_{CR} using the transport scattering times ($\tau_s \approx \tau_{DC} = m^*\mu_{dc}/e \approx 140$ ps), which we find cannot reproduce the full temperature dependence from 0.4 to 100 K of τ_{CR} in our sample. Figure 3(b) shows a simulation of τ_{DC} (solid line) using the model developed for two-dimensional gallium arsenide systems in Ref. [42]. The contributions to τ_{DC} include polar optical phonon scattering (τ_{PO}, dot-dashed line), piezoelectric scattering (τ_{PZ}, dotted line), acoustic deformation potential scattering (τ_A, long- and short-dashed line), and impurity scattering (τ_i, dashed line) [42] and reproduce τ_{DC} at 4.2 K (triangles). At the highest temperatures studied, τ_{CR} is limited by polar optical phonon scattering and, as noted above,

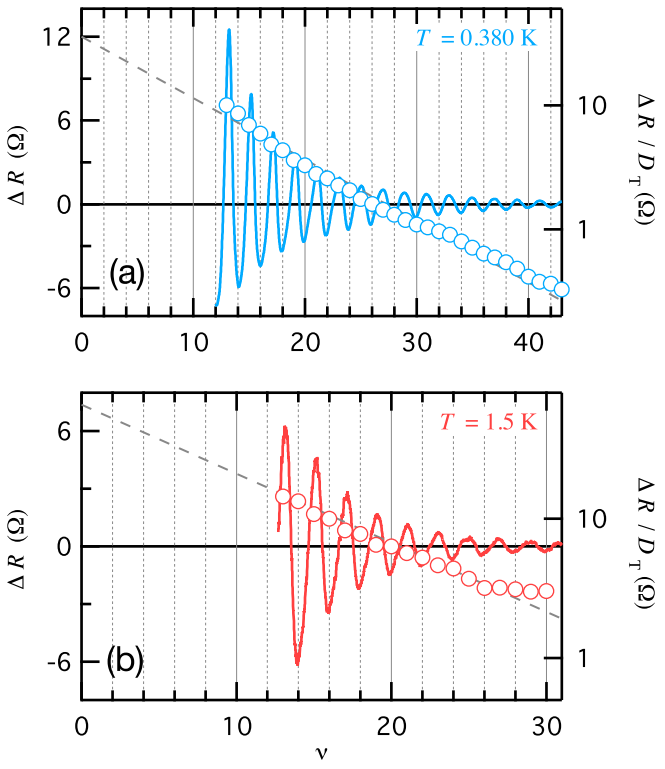

FIG. 4. Left axis: Magnetoresistance ΔR of the sample at (a) 0.380 K (b) and 1.5 K. Right axis: The reduced oscillation amplitude $\Delta R/D_{\mathrm{T}}$ versus filling factor ν from which we determine a quantum time, $\tau_q = 1.1$ ps.

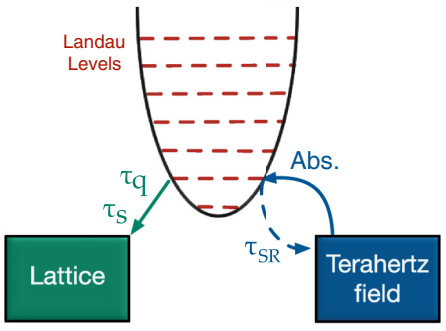

FIG. 5. A three-interacting-systems model of this experiment. The Landau levels, induced by the perpendicular magnetic field on the 2DEG, are coupled to the terahertz field (absorption and superradiance) and to the lattice (scattering).

results in the concomitant decrease in amplitude above 50 K. Using this τ_{DC} model for τ_s predicts a temperature dependence for τ_{CR} below 50 K that is not consistent with our data, with a τ_{DC} that is much longer (solid line) than our τ_s (squares). The modification of the density of states near E_F, however, results in a reduction in the relevant scattering times (i.e., $\tau_s < \tau_{DC}$) in the 2DEG [13,14]. At the lowest temperatures, a scattering contribution to τ_{CR} would be determined by both impurity scattering and acoustic deformation potential scattering, which is at least a component of the temperature dependence of τ_s.

The reduction in amplitude shown in Fig. 3(a) may indicate a reduction in n_s below ∼1.5 K, resulting in a spectral weight transfer away from $h\nu_c$. If we assume no change to $|\hat{d}|^2$, then the reduction in A would be a direct measure of the reduction in n_s. Since Eq. (4b) describes an inverse relationship for $\tau_{SR} \sim n_s^{-1}$, this reduction in n_s would be at least a component of the *increase* the cyclotron decay time over the same temperature range. From 1.5 to 0.4 K the amplitude is reduced by ∼2.5 times, while the corresponding increase in decay time is only 1.6 times. This scenario for $\tau_s(T)$ thus cannot alone explain our results from 0.4 to 1.5 K. It is likely that a combination of dissipative and radiative processes can successfully explain our observed data (squares), but further experiments that fully measure and model the B and T dependence of τ_{CR} will be needed.

The difference between $\tau_q = 1.1$ ps and $\tau_s = 66.4$ ps $\approx 60 \times \tau_q$ at low temperatures in this sample highlights the importance of small-angle scattering in this high-mobility 2DEG. Using the relaxation-time approximation, the scattering time τ measured in a given experimental geometry is given by

$$\frac{1}{\tau} = \int W(\vec{k},\vec{k}')f(\theta)d\vec{k}, \tag{5}$$

where $W(\vec{k},\vec{k}')$ is the scattering probability for an electron in $\vec{k}$ to scatter into $\vec{k}'$, θ is the angle between $\vec{k}$ and $\vec{k}'$, and $f(\theta)$ is a weight function that determines the relative contribution to τ for each scattering angle. The measured $\tau_{DC} = 140$ ps, for example, is primarily determined by large-angle scattering from long-range scattering since $\tau_{DC} \gg \tau_q$. From the relevant Boltzmann equation, τ_{DC} is weighted by $f(\theta) = (1 - \cos\theta)$, which suppresses small-angle scattering contributions. In contrast, τ_q in homogeneous samples has $f(\theta) = 1$ and is a determined by the full $W(\vec{k},\vec{k}')$, as has been discussed previously [6,24,51,52]. In *homogeneous* samples, τ_q is closely related to the dissipative component cyclotron decay time τ_s. Disagreement between τ_s and τ_{CR}, as we observe in our data, has been previously attributed to disorder in samples with lower mobilities ($\mu \lesssim 10^4$ cm^2 V^{-1} s^{-1}) [51,52]. A spatial variation in the carrier concentration $\Delta n_s(x,y)$ within the two-dimensional layer results in an apparent reduction in τ_q due to the resulting spatial variation in E_F. The resistance oscillations seen in Fig. 4 have minima that are located at even integral multiples of the filling factor ν, which result from edge-channel conduction in the sample. A spatial variation in n_s would correspond to different values of E_F, changing the B fields where these resistance minima occur, which is known to lead to a reduction in the apparent τ_q [52]. The carrier concentration variation needed to explain the discrepancy between $\tau_s = 66.4$ ps and $\tau_q = 1.1$ ps in our sample would be on the order of $\frac{\Delta n_s}{n_s} \sim 15\%$ [51]. In our sample, this carrier concentration variation is fundamentally inconsistent with the sample mobility of $\mu_{dc} = 3.6 \times 10^6$ cm^2 V^{-1} s^{-1}, which has previously been found to occur in samples with low defect density, atomically smooth interfaces, and otherwise homogenous properties [6]. The difference between τ_s and τ_q has been previously predicted and results from the importance of small-angle scattering in this high-mobility sample. A significant role for small-angle scattering in this sample is consistent with the ratio of the quantum and transport lifetimes, $\tau_q/\tau_{DC} \ll 1$, in our sample [52]. Small-angle scattering with an angle θ between k and k' will not significantly contribute to dephasing below a critical angle $\theta_c \lessapprox \pi/(2\nu) \leqslant 13^\circ$, determined by the filling factor ν [51,53]. The scattering rate τ^{-1}, determined by Eq. (5), cannot be used directly to calculate τ_s, which only has contributions from a subset of scattering events when $\theta > \theta_c$.

V. CONCLUSIONS

In summary, we have performed cyclotron resonance spectroscopy in a Landau-quantized two-dimensional electron gas with a high mobility of $\mu_{dc} = 3.6 \times 10^6$ cm^2 V^{-1} s^{-1} and a carrier concentration of $n_s = 2 \times 10^{10}$ cm^{-2}. We find a cyclotron resonance decay time τ_{CR} that decreases monotonically as temperature increases from 0.4 to 100 K, which results both from the contribution from superradiance and from a temperature-dependent contribution. Shubnikov–de Haas characterization of this sample determines a quantum lifetime, $\tau_q = 1.1$ ps, which is ∼60 times faster than the corresponding τ_s, which we attribute to the importance of the small-angle scattering $\theta \leqslant 13^\circ$ contribution to τ_q and not to cyclotron dephasing. The reduction in both oscillation amplitude and lifetime above 50 K is the result of the onset of strong polar optical phonon scattering. The temperature-dependent τ_s below 1.5 K may be the result of dissipative mechanisms (impurity scattering and acoustic deformation potential scattering) and/or from a reduction in carrier concentration n_s that would result in an increase in the superradiant decay time. The origin of this potential reduction in oscillation amplitude/carrier concentration at low temperatures is currently unclear and will be the focus of future studies.

ACKNOWLEDGMENTS

This material is based upon work supported by the National Science Foundation under Grants No. DMR-1056827 (J.A.C., T.T., and D.J.H.) and No. DMR-1409473 (D.K.). J.A.C. also acknowledges support from the U.S. Department of Education GAANN Fellowship (P200A090143). A.T.H. acknowledges L. W. Engel for support and use of equipment for the SdHO measurements. A portion of this work was performed at the National High Magnetic Field Laboratory, which is supported by National Science Foundation Cooperative Agreement No. DMR-1157490 and the state of Florida. This work was performed, in part, at the Center for Integrated Nanotechnologies, a U.S. Department of Energy, Office of Basic Energy Sciences, user facility. Sandia National Laboratories is a multiprogram laboratory managed and operated by Sandia Corporation, a wholly owned subsidiary of Lockheed Martin Corporation, for the U.S. Department of Energy's National Nuclear Security Administration under Contract No. DE-AC04-94AL85000.

[1] T. Ando, A. B. Fowler, and F. Stern, Electronic properties of two-dimensional systems, Rev. Mod. Phys. **54**, 437 (1982).

[2] B. J. F. Lin, D. C. Tsui, M. A. Paalanen, and A. C. Gossard, Mobility of the two-dimensional electron gas in GaAs-$Al_xGa_{1-x}As$ heterostructures, Appl. Phys. Lett. **45**, 695 (1984).

[3] J. J. Harris, C. T. Foxon, D. Hilton, J. Hewett, C. Roberts, and S. Auzoux, Acoustic phonon scattering in ultra-high mobility, low carrier density GaAs/(Al,Ga)As heterojunctions, Surf. Sci. **229**, 113 (1990).

[4] O. E. Dial, R. C. Ashoori, L. N. Pfeiffer, and K. W. West, High-resolution spectroscopy of two-dimensional electron systems, Nature (London) **448**, 176 (2007).

[5] T. Champel, S. Florens, and L. Canet, Microscopics of disordered two-dimensional electron gases under high magnetic fields: Equilibrium properties and dissipation in the hydrodynamic regime, Phys. Rev. B **78**, 125302 (2008).

[6] S. Das Sarma, E. H. Hwang, S. Kodiyalam, L. N. Pfeiffer, and K. W. West, Transport in two-dimensional modulation-doped semiconductor structures, Phys. Rev. B **91**, 205304 (2015).

[7] Y. Ji, Y. Chung, D. Sprinzak, M. Heiblum, D. Mahalu, and H. Shtrikman, An electronic Mach Zehnder interferometer, Nature (London) **422**, 415 (2003).

[8] L. V. Litvin, A. Helzel, H. P. Tranitz, W. Wegscheider, and C. Strunk, Edge-channel interference controlled by Landau level filling, Phys. Rev. B **78**, 075303 (2008).

[9] A. Sarkar, T. K. Bhattacharyya, and A. Patwardhan, Quantum logic processor: Implementation with electronic Mach-Zehnder interferometer, Appl. Phys. Lett. **88**, 213113 (2006).

[10] N. H. Bonadeo, J. Erland, D. Gammon, D. Park, D. S. Katzer, and D. G. Steel, Coherent optical control of the quantum state of a single quantum dot, Science **282**, 1473 (1998).

[11] T. Arikawa, X. Wang, David J. Hilton, J. L. Reno, W. Pan, and J. Kono, Quantum control of a Landau-quantized two-dimensional electron gas in a GaAs quantum well using coherent terahertz pulses, Phys. Rev. B **84**, 241307 (2011).

[12] Q. Zhang, T. Arikawa, E. Kato, J. L. Reno, W. Pan, J. D. Watson, M. J. Manfra, M. A. Zudov, M. Tokman, M. Erukhimova, A. Belyanin, and J. Kono, Superradiant Decay of Cyclotron Resonance of Two-Dimensional Electron Gases, Phys. Rev. Lett. **113**, 047601 (2014).

[13] C. K. Sarkar and R. J. Nicholas, Cyclotron resonance linewidth in a two-dimensional electron gas, Surf. Sci. **113**, 326 (1982).

[14] M. A. Hopkins, R. J. Nicholas, D. J. Barnes, M. A. Brummell, J. J. Harris, and C. T. Foxon, Temperature dependence of the cyclotron-resonance linewidth in GaAs-$Ga_{1-x}Al_xAs$ heterojunctions, Phys. Rev. B **39**, 13302 (1989).

[15] J. M. Luttinger, Quantum Theory of Cyclotron Resonance in Semiconductors: General Theory, Phys. Rev. **102**, 1030 (1956).

[16] Th. Englert, J. C. Maan, Ch. Uihlein, D. C. Tsui, and A. C. Gossard, Observation of oscillatory line width in the cyclotron resonance of GaAs-AlGaAs heterostructures, Solid State Commun. **46**, 545 (1983).

[17] Z. Schlesinger, W. Wang, and A. H. MacDonald, Dynamical Conductivity of the GaAs Two-Dimensional Electron Gas at Low Temperature and Carrier Density, Phys. Rev. Lett. **58**, 73 (1987).

[18] M. Chou, D. Tsui, and G. Weimann, Cyclotron resonance of high-mobility two-dimensional electrons at extremely low densities, Phys. Rev. B **37**, 848 (1988).

[19] T. Morimoto, Y. Hatsugai, and H. Aoki, Optical Hall Conductivity in Ordinary and Graphene Quantum Hall Systems, Phys. Rev. Lett. **103**, 116803 (2009).

[20] V. Fock, Bemerkung zur Quantelung des harmonischen Oszillators im Magnetfeld, Z. Phys. **47**, 446 (1928).

[21] C. Cohen-Tannoudji, B. Diu, and F. Laloe, *Quantum Mechanics* (Wiley, New York, 1978), Vol. 1.

[22] W. Seidenbusch, E. Gornik, and G. Weinmann, Cyclotron-resonance linewidth oscillations in the integer and fractional quantum Hall regimes, Phys. Rev. B **36**, 9155 (1987).

[23] H. Sigg, P. Wyder, and J. A. A. J. Perenboom, Analysis of polaron effects in the cyclotron resonance of n-GaAs and AlGaAs-GaAs heterojunctions, Phys. Rev. B **31**, 5253 (1985).

[24] I. V. Andreev, V. M. Muravev, V. N. Belyanin, and I. V. Kukushkin, Measurement of cyclotron resonance relaxation time in the two-dimensional electron system, Appl. Phys. Lett. **105**, 202106 (2014).

[25] *Sensing with Terahertz Radiation*, edited by D. Mittleman (Springer, Berlin, 2002).

[26] D. Some and A. V. Nurmikko, Real-time electron cyclotron oscillations observed by terahertz techniques in semiconductor heterostructures, Appl. Phys. Lett. **65**, 3377 (1994).

[27] X. Wang, D. J. Hilton, L. Ren, D. M. Mittleman, J. Kono, and J. L. Reno, Terahertz time-domain magnetospectroscopy of a high-mobility two-dimensional electron gas, Opt. Lett. **32**, 1845 (2007).

[28] J. Lloyd-Hughes, H. E. Beere, D. A. Ritchie, and M. B. Johnston, Terahertz magnetoconductivity of excitons and electrons in quantum cascade structures, Phys. Rev. B **77**, 125322 (2008).

[29] D. J. Hilton, Cyclotron resonance spectroscopy in a high mobility two dimensional electron gas using characteristic matrix methods, Opt. Express **20**, 29717 (2012).

[30] N. Kamaraju, W. Pan, U. Ekenberg, D. M. Gvozdić, S. Boubanga-Tombet, P. C. Upadhya, J. Reno, A. J. Taylor, and R. P. Prasankumar, Terahertz magneto-optical spectroscopy of a two-dimensional hole gas, Appl. Phys. Lett. **106**, 031902 (2015).

[31] A. Nahata, A. S. Weling, and T. F. Heinz, A wideband coherent terahertz spectroscopy system using optical rectification and electro-optic sampling, Appl. Phys. Lett. **69**, 2321 (1996).

[32] Q. Chen, M. Tani, Z. Jiang, and X.-C. Zhang, Electro-optic transceivers for terahertz-wave applications, J. Opt. Soc. Am. B **18**, 823 (2001).

[33] M. van Exter, Ch. Fattinger, and D. Grischkowsky, Terahertz time-domain spectroscopy of water vapor, Opt. Lett. **14**, 1128 (1989).

[34] C. R. Brundle, C. A. Evans, and S. Wilson, *Encyclopedia of Materials Characterization: Surfaces, Interfaces, Thin Films* (Gulf Professional Publishing, Boston, 1992).

[35] O. Morikawa, A. Quema, S. Nashima, H. Sumikura, T. Nagashima, and M. Hangyo, Faraday ellipticity and Faraday rotation of a doped-silicon wafer studied by terahertz time-domain spectroscopy, J. Appl. Phys. **100**, 033105 (2006).

[36] S. E. Ralph, S. Perkowitz, N. Katzenellenbogen, and D. Grischkowsky, Terahertz spectroscopy of optically thick multilayered semiconductor structures, J. Opt. Soc. Am. B **11**, 2528 (1994).

[37] M. Born and E. Wolf, *Principles of Optics: Electromagnetic Theory of Propagation, Interference and Diffraction of Light*, 7th ed. (Cambridge University Press, Cambridge, 1999).

[38] L. Duvillaret, F. Garet, and J.-L. Coutaz, A Reliable Method for Extraction of Material Parameters in Terahertz Time-Domain Spectroscopy, IEEE J. Sel. Top. Quantum Electron. **2**, 739 (1996).

[39] R. W. Boyd, *Nonlinear Optics*, 3rd ed. (Academic, Amsterdam, 2008).

[40] J. W. Goodman, *Introduction To Fourier Optics*, 2nd ed. (McGraw-Hill, New York, 1996).

[41] In SI units, the polarization is given in the usual form with $P(\nu) = \epsilon_0 \tilde{\chi}(\nu) E(\nu)$ in the frequency domain and $P(t) = R(t) \otimes E(t)$ in the time domain, where $\otimes$ is the convolution operator.

[42] K. Lee, M. S. Shur, T. J. Drummond, and H. Morkoç, Low field mobility of 2-d electron gas in modulation doped $Al_xGa_{1-x}As$/GaAs layers, J. Appl. Phys. **54**, 6432 (1983).

[43] S. Adachi, GaAs, AlAs, and $Al_xGa_{1-x}As$ Material parameters for use in research and device applications, J. Appl. Phys. **58**, R1 (1985).

[44] L. V. Shubnikov and W. J. de Haas, Proc. Net. R. Acad. Sci. **207a**, 13 (1930).

[45] P. T. Coleridge, Small-angle scattering in two-dimensional electron gases, Phys. Rev. B **44**, 3793 (1991).

[46] T. Kawamura and S. Das Sarma, Phonon-scattering-limited electron mobilities in $Al_xGa_{1-x}As$/GaAs heterojunctions, Phys. Rev. B **45**, 3612 (1992).

[47] In contrast, $\tilde{\chi}_0$ depends linearly on $N|\hat{d}|^2\tau_{CR}$ and is approximately constant over the same temperature range.

[48] R. Dingle, H. L. Störmer, A. C. Gossard, and W. Wiegmann, Electron mobilities in modulation-doped semiconductor heterojunction superlattices, Appl. Phys. Lett. **33**, 665 (1978).

[49] H. P. Breuer and F. Petruccione, *The Theory of Open Quantum Systems* (Oxford University Press, Oxford, 2002).

[50] R. H. Dicke, Coherence in Spontaneous radiation processes, Phys. Rev. **93**, 99 (1954).

[51] J. P. Harrang, R. J. Higgins, R. K. Goodall, P. R. Jay, M. Laviron, and P. Delescluse, Quantum and classical mobility determination of the dominant scattering mechanism in the two-dimensional electron gas of an AlGaAs/GaAs heterojunction, Phys. Rev. B **32**, 8126 (1985).

[52] S. Syed, M. J. Manfra, Y. J. Wang, R. J. Molnar, and H. L. Störmer, Electron scattering in AlGaN/GaN structures, Appl. Phys. Lett. **84**, 1507 (2004).

[53] D. W. Terwilliger and R. J. Higgins, Dislocations and the de Haas–van Alphen Effect in Copper, Phys. Rev. B **7**, 667 (1973).